Earth and Planetary Science Letters 388 (2014) 9–17

Contents lists available at ScienceDirect

Earth and Planetary Science Letters

www.elsevier.com/locate/epsl

Nonrandom geomagnetic reversal times and geodynamo evolution

Peter Olson [a,*], Linda A. Hinnov [a], Peter E. Driscoll [b]

[a] Department of Earth and Planetary Sciences, Johns Hopkins University, Baltimore, MD, USA
[b] Department of Geology and Geophysics, Yale University, New Haven, CT, USA

ARTICLE INFO

Article history:
Received 17 June 2013
Received in revised form 15 November 2013
Accepted 18 November 2013
Available online 13 December 2013
Editor: Y. Ricard

Keywords:
geodynamo
polarity reversals
Geomagnetic Polarity Time Scale
superchrons
Sherman's test

ABSTRACT

Sherman's ω-test applied to the Geomagnetic Polarity Time Scale (GPTS) reveals that geomagnetic reversals in the Phanerozoic deviate substantially from random times. For 954 Phanerozoic reversals, ω exceeds the value expected for uniformly distributed random times by many standard deviations, due to three constant polarity superchrons and clustering of reversals in the Cenozoic C-sequence. Reversals are nearly periodic in several portions of the Mesozoic M-sequence, and during these times ω falls below random by several standard deviations, according to some chronologies. Polarity reversals in a convection-driven numerical dynamo with fixed control parameters have an overall ω-value that is slightly lower than uniformly random due to weak periodicity, whereas in a numerical dynamo with time-variable control parameters the combination of superchrons and reversal clusters dominates, yielding a large ω-value that is comparable to the GPTS. Sherman's test applied to shorter Phanerozoic reversal sequences reveals two geodynamo time scales: hundreds of millions of years represented by superchrons and reversal clusters that we attribute to time-dependent core–mantle thermal interaction, plus unexplained variations lasting tens of millions of years characterized by alternation between random and nearly periodic reversals.

1. Introduction

Identifying the causes of time variability of geomagnetic polarity reversals is fundamental to understanding the geodynamo. The time between geomagnetic reversals varies over more than three orders of magnitude, from 40 Myr constant polarity superchrons to short chrons of a few tens of thousands of years (Ogg, 2012) and even shorter polarity excursion events lasting a few thousand years (Valet et al., 2008). This behavior contrasts with the solar dynamo, which reverses polarity regularly with each solar cycle, creating a nearly periodic 22-yr dynamo oscillation (Jones et al., 2010).

Because of their variability, most analyses of geomagnetic reversal sequences treat individual reversals as random events and seek a statistical characterization of their frequency. A standard approach is to compare the distribution of geomagnetic polarity chron lengths to well-known probability distributions, such as Poisson, gamma, or log-normal. There is a long-running controversy about which probability distribution best represents geomagnetic reversal sequences, and what it implies for the geodynamo (Naidu, 1971; Phillips, 1977; McFadden and Merrill 1984; 1997; Constable, 2000; Sorriso-Valvo et al., 2007; Ryan and Sarson, 2007; Vallianatos, 2011; Shcherbakov and Fabian, 2012).

Numerical dynamos offer a powerful tool for interpreting reversal sequences in terms of the fundamental dynamical processes that govern the geodynamo (Glatzmaier et al., 1999). Convection-driven numerical dynamos have been run for the equivalent of hundreds of millions of years in low resolution mode, producing continuous reversal sequences numbering in the hundreds (Wicht et al. 2009; 2010; Driscoll and Olson, 2011; Lhuillier et al., 2013). Direct comparisons have been made between histograms of chron lengths generated by numerical dynamos and the Poisson and other probability distributions (Lhuillier et al., 2013), between dynamo and geomagnetic reversal sequences in the time domain (Driscoll and Olson, 2011; Olson et al., 2013), and between individual geomagnetic and dynamo reversals (Amit et al., 2010; Olson et al., 2011), with fair agreement in some cases. Overall, the variety of reversals in these dynamos (Wicht and Olson, 2004; Aubert et al., 2008; Wicht et al., 2009; Olson et al., 2010) is comparable to the variety in the paleomagnetic record (Valet et al., 2012).

Reversals in numerical dynamos can be divided into three broadly defined categories, based on their sequencing. First, there are dynamos that produce sequences of regularly spaced reversals. Typically, these dynamos are rich in large-scale shear flows (Wicht and Olson, 2004). In this paper we use the term *periodic* for reversal sequences of this type, even though their polarity chrons are generally not precisely equal in length. Second, there are dynamos that produce seemingly random reversal sequences. Much of the kinetic energy in these dynamos is concentrated in

* Corresponding author.
E-mail address: olson@jhu.edu (P. Olson).

0012-821X/$ – see front matter
http://dx.doi.org/10.1016/j.epsl.2013.11.038

smaller-scale convection (Aubert et al., 2008) rather than larger-scale shear flows. Reversal times in these dynamos appear to be uniformly probable (Lhuillier et al., 2013), although there may be inhibition for a short time immediately following a reversal (Wicht et al., 2010). We use the term *random* for reversal sequences of this type. The third category includes numerical dynamos with strongly modulated external forcing, such as time variable core–mantle boundary heat flow and variable rotation. These dynamos tend to produce reversal sequences modulated on the timescales of the external forcing (Driscoll and Olson, 2009b) and may show long intervals with stable polarity analogous to geomagnetic superchrons, as well as dense clusters of reversals. In conformity with previous studies (Jonkers, 2003; Carbone et al., 2006) we use the term *clustered* for reversal sequences of this type.

Here we analyze the entire Phanerozoic Geomagnetic Polarity Time Scale (GPTS) as well as Cenozoic and Mesozoic portions of the GPTS using Sherman's ω-test, finding evidence of periodic, random, and clustered behavior. We apply the same analysis to long reversal sequences from two convection-driven numerical dynamos, one with fixed (time-independent) control parameters, the other with modulated (time-dependent) control parameters that is meant to simulate the evolution of the geodynamo caused by changes in the dynamical state of the core. We show that the dynamo with modulated core parameters yields ω-statistics similar to the Phanerozoic GPTS, whereas the dynamo with fixed parameters does not.

2. Sherman's test for random times

Sherman (1950) proposed the following statistic to measure deviations from uniform spacing in a sequence of n events that occur at discrete times t_i:

$$\omega_n = \frac{1}{2\tau}\sum_{i=1}^{n+1}\left|x_i - \frac{\tau}{n+1}\right| \tag{1}$$

where x_i denotes the $n+1$ time intervals separating the events, and

$$\tau = \sum_{i=1}^{n+1} x_i \tag{2}$$

is the total duration of the record. Because the second term on the r.h.s. of (1) represents the average time interval, ω_n is a simple measure of how much the $n+1$ intervals deviate from their average length. In our application, t_i represent the reversal times (chron boundaries), x_i are the chron lengths, and τ is the length of the record under consideration.

Use of absolute values in the definition of statistical parameters often causes mathematical problems, but in this case Sherman (1950; 1957) has shown that the moments and percentiles of (1) can be calculated in finite terms. In particular, the mean μ_n and the variance σ_n^2 of ω_n for n uniformly distributed random events are given by

$$\mu_n = \left(\frac{n}{n+1}\right)^{n+1} \tag{3}$$

and

$$\sigma_n^2 = \frac{2n^{n+2} + n(n-1)^{n+2}}{(n+2)(n+1)^{n+2}} - \left(\frac{n}{n+1}\right)^{2n+2} \tag{4}$$

respectively. For a large number of events ($n \gg 1$), (3) and (4) simplify to

$$\mu_n \simeq e^{-1} \tag{5}$$

and

$$\sigma_n^2 \simeq \frac{2e-5}{ne^2}, \tag{6}$$

respectively. In this same limit, the standardized variable

$$\omega_n^* = \frac{\omega_n - \mu_n}{\sigma_n} \tag{7}$$

approaches a Normal distribution with zero mean and variance one. According to (1), the range of ω_n is given by

$$0 \leqslant \omega_n \leqslant \frac{n}{n+1}, \tag{8}$$

the lower limit of $\omega_n = 0$ corresponding to events that are equally spaced in time, and the upper limit of $\omega_n = 1$ corresponding to $n \gg 1$ events that are tightly clustered in time. Uniformly random times yield a value of $\omega_n = 1/e \simeq 0.3679$ for $n \gg 1$, according to (3) and (5).

The clear separation between the limiting values of ω_n provides a straight-forward way to analyze and interpret reversal sequences in the GPTS and numerical dynamos, by classifying reversal sequences as periodic (nearly equal chron lengths and $\omega_n \ll 1/e$), uniformly random (moderately variable chron lengths and $\omega_n \simeq 1/e$), or clustered (extremely variable chron lengths and $\omega_n \gg 1/e$). Furthermore, likelihoods can be assigned to these classifications using (3) and (4), even for sequences with a relatively small number of reversals. In Appendix A we give exact and approximate expressions for calculating P, the percentiles of Sherman's ω that correspond to uniformly random times, along with tabulated values of P for small and moderate sample sizes n.

3. Sherman's test applied to Phanerozoic reversals

Fig. 1 shows the sequence of geomagnetic reversals for the Phanerozoic Eon from Ogg (2012), in terms of the polarity, the five million year running average reversal rate, and the average polarity bias ($f_N - f_R$), where f_N and f_R denote the fraction of time spent in normal and reverse polarity, respectively. The Phanerozoic reversal record is known to be incomplete, particularly in the Paleozoic, and in addition, there are uncertainties in the timings of individual reversals, especially those older than the Cenozoic C-sequence (Cande and Kent, 1995; Ogg, 2012). Accordingly, we also analyze two other recent compilations of Mesozoic M-sequences (Tominaga and Sager, 2010; Malinverno et al., 2012). Table 1 gives n, ω_n, ω_n^* and P for the five GPTS sequences considered.

For the 0–542 Ma Phanerozoic GPTS, we find $\omega_n = 0.558$. For $n = 954$ random times, $\mu_n \simeq 1/e$ and $\sigma_n \simeq 7.9 \times 10^{-3}$, so the Phanerozoic ω is about 24 standard deviations above random, as Table 1 shows. The primary cause of the anomalously large ω in the Phanerozoic is the slow modulation in reversal frequency evident in Fig. 1, and in particular, the three constant polarity superchrons, the Cretaceous Normal Superchron (CNS) at 83–125 Ma, the Kiaman Reversed Superchron (KRS) at 267–314 Ma, and the Moyero Reversed Superchron (MRS) at 463–482 Ma (Pavlov and Gallet, 2005), intervals devoid of (or nearly devoid of) reversals that are far too long to have occurred by chance alone. This inference is fully consistent with previous interpretations of reversals as outcomes of a Poisson or a gamma process. For example, if we were to assume that geomagnetic reversal times obey either Poisson (Phillips, 1977) or gamma statistics (McFadden, 1984) with a mean reversal rate of 2 per million years, then it is easy to show that the likelihood of three constant polarity superchrons occurring within the Phanerozoic by chance alone is vanishingly small.

The statistics in Table 1 also reveal that geomagnetic reversals deviate from uniformly random times away from the superchrons. For example, Table 1 shows that $\omega_n = 0.409$ for GPTS reversals

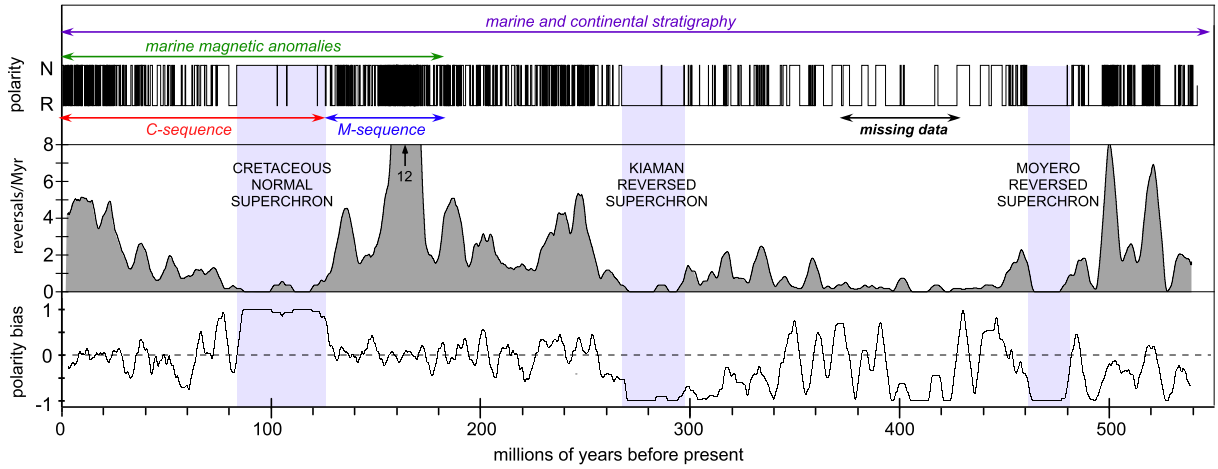

Fig. 1. Reversal sequences from the Geomagnetic Polarity Time Scale (GPTS). Top: Phanerozoic polarity sequence 0–542 Ma from Ogg (2012) with Cenozoic (C) and Mesozoic (M) sequences; N = normal, R = reverse. Middle: Phanerozoic polarity reversal rate, 5 Myr running average. Bottom: polarity bias, 5 Myr running average; +1 = normal, −1 = reverse.

Table 1
Sherman statistics for geomagnetic and dynamo reversals.

Sequence	ID	Time span	Reversals, n	ω_n	ω_n^*	P (%)
Phanerozoic	PO	0–542 Ma	954	0.5581	+24	99.9
C-sequence	CO	0–62 Ma	170	0.4091	+2.3	98.7
M-sequence	MO	122–158 Ma	102	0.3923	+1.0	86.2
M-sequence	MTS	124–158 Ma	101	0.3045	−2.6	0.44
M-sequence	MHTC	121–156 Ma	101	0.2690	−4.2	0.002
Fixed dynamo	F50	50 Myr	100	0.3310	−1.5	7.2
Evolving dynamo	E200	200 Myr	478	0.4761	+9.4	99.9
Evolving dynamo	E80	80 Myr	239	0.4094	+2.6	99.6
Evolving dynamo	E50	50 Myr	105	0.4017	+1.5	93.3

PO, CO, MO = Ogg (2012); MTS = Tominaga and Sager (2010); MHTC = Malinverno et al. (2012); F50, E200, E80, E50 = Driscoll and Olson (2009a, 2011).

in the Cenozoic C-sequence during the interval 0–62 Ma, which exceeds the value expected for $n = 170$ uniformly random times by approximately 2.3 standard deviations. We can therefore infer with 98% confidence that polarity reversals since 62 Ma show clustering. This result supports previous studies that analyzed the overall increase in reversal frequency since the CNS (Lowrie and Kent, 1983; Gallet and Courtillot, 1995; Gallet and Hulot, 1997; Sorriso-Valvo et al., 2007) and came to similar conclusions.

The timing for older reversal sequences is less certain, but nevertheless shows additional evidence for deviations from randomness at some times. Fig. 2 shows three compilations of the youngest portion of the Mesozoic M-sequence: MTS by Tominga and Sager (2010), MHTC by Malinverno et al. (2012), and MO from Ogg (2012). Rather different crustal age interpolations were used in each of these compilations. For MO, Ogg (2012) applied linear interpolations between fixed age points. For MHTC, Malinverno et al. (2012) interpolated between sea floor magnetic anomalies of known dates by minimizing global variations in spreading rates. For MTS, Tominaga and Sager (2010) assumed constant ratios of spreading rates among three sets of magnetic lineations in the Pacific. As a result, the spreading rates that underlie MHTC and MTS are inherently smoother than MO, and these smoothings produce more regularity in their estimates of the reversal times. As shown in Table 1, ω_n is about one standard deviation above random for the MO sequence, whereas it is 2.6 and 4.2 standard deviations below random for the MTS and MHTC sequences, respectively. In particular, the global minimization of sea floor spreading rate variations applied by Malinverno et al. (2012) results in highly regular (that is, almost periodic) reversal times during 121–156 Ma.

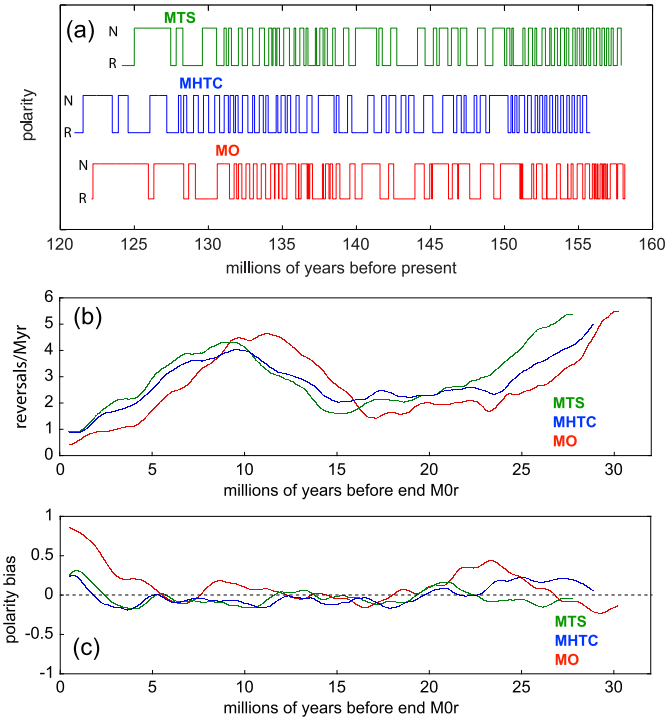

Fig. 2. Mesozoic reversal sequences comparison. (a) Polarity sequences starting from reversal M0r. Sequence labeled MTS is from Tominaga and Sager (2010), sequence labeled MHTC is from Malinverno et al. (2012), and sequence labeled MO is from Ogg (2012). (b) Polarity reversal rates for each sequence, 5 Myr running average. (c) Polarity bias for each sequence, 5 Myr running average.

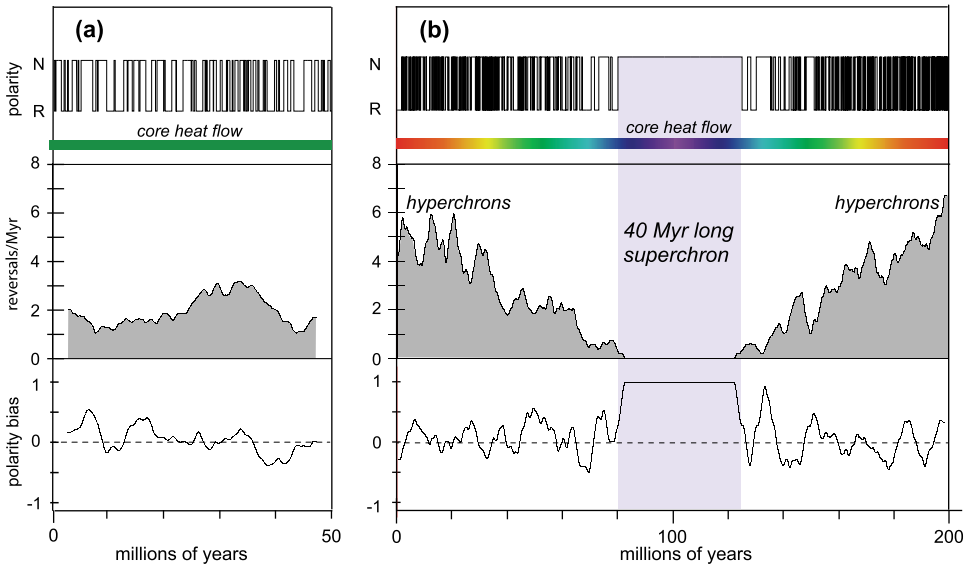

Fig. 3. (a) Reversals in numerical dynamo with fixed control parameters. Top: polarity sequence; middle: polarity reversal rate, 5 Myr running average; bottom: polarity bias, 5 Myr running average. (b) Reversals in numerical dynamo with evolving control parameters. Top: polarity sequence; middle: polarity reversal rate, 5 Myr running average; bottom: polarity bias, 5 Myr running average. Color bar shows relative variation in core–mantle boundary heat flow (red, purple = 1.4, 0.7 times green, respectively.) (For interpretation of the references to color in this figure legend, the reader is referred to the web version of this article.)

4. Sherman's test applied to dynamo reversals

The existence of clustered, periodic, and random reversal sequences at separate times in the GPTS could possibly be interpreted in terms of a geodynamo process which is stationary in time but with a long-range organization that produces low-frequency deviations from Poisson or gamma reversal statistics and the occasional constant polarity superchron (Jonkers, 2007; Ryan and Sarson, 2007; Vallianatos, 2011). The alternative interpretation is that these slow GPTS variations signify that the dynamical states of the core and the geodynamo are not stationary, but instead fluctuate on long time scales, possibly due to time variations in the energy balance of the core, time variations in mantle forcing, or some combination. For example, Lowrie and Kent (2004) have argued that the systematic trend toward lower reversal frequency with age in the C-sequence (0–123 Ma) in Fig. 1 is a result of non-stationary behavior in the geodynamo process. Likewise, Glatzmaier et al. (1999), Courtillot and Olson (2007), and Olson et al. (2013) have proposed that reversal modulations are driven by variability in core–mantle boundary heat flow, and Biggin et al. (2012) have suggested that true polar wander events contribute to reversal modulation. In contrast, Hulot and Gallet (2003) and Aubert et al. (2009) have argued that the geodynamo can produce occasional superchrons without changing the state of the core.

As a test of these competing interpretations, we calculate Sherman statistics for sequences of reversals from numerical dynamos with both fixed and time-variable control parameters, and compare these with Sherman statistics from the GPTS. Fig. 3a shows a sequence of reversals from a numerical dynamo driven by thermochemical convection similar to those described in Driscoll and Olson (2009a), with the following fixed (time-independent) control parameters: Rayleigh number $= 4 \times 10^4$, Ekman number $= 5.75 \times 10^{-3}$, magnetic Prandtl number $= 20$, Prandtl number $= 1$, and a volumetric buoyancy sink term of unit strength. The boundary conditions are also fixed, in particular, the core–mantle boundary heat flow is spatially uniform and constant in time. Time is scaled by assuming a dipole magnetic diffusion time of 20 kyr and progresses from right to left in Fig. 3a, in conformity with Fig. 1. This dynamo produced 100 reversals in 50 Myr of simulated time, consistent with the overall rate in the Phanerozoic, with 5 Myr average reversal rates varying from about 1 to 3 Myr^{-1}. Interestingly, there is some visual suggestion of a slow modulation in the polarity sequence, the reversal rate, and in the polarity bias. Nevertheless, the results of Sherman's test in Table 1 show that $\omega_n = 0.331$ for the complete sequence of $n = 100$ reversals of this dynamo, which is far too low for reversal clustering, and in fact is about 1.5 standard deviations lower than what is expected for uniformly random times. The explanation for this behavior is two-fold. First, there are no long stable polarity intervals in this dynamo that are comparable to the superchrons in the Phanerozoic GPTS. Second, although there is some suggestion of clusters within the reversal sequence, there are also intervals when the reversal times are nearly equally spaced, that is, periodic reversals. For this dynamo, the periodic reversal sequences have a greater influence on ω than does the weak clustering.

The statistics change dramatically when core evolution is added to the numerical dynamo. Fig. 3b shows the sequence of reversals from a numerical dynamo (Driscoll and Olson, 2011) in which the magnitude of the core–mantle boundary heat flow is varied with a 200 Myr periodicity. The time average core–mantle boundary heat flow for this dynamo is the same as the time-independent value in the previous case (Fig. 3b), and the amplitude (peak-to-peak) of variation is 40% of this average. The other control parameters of the two dynamos are identical. As several previous dynamo studies have found, increasing the heat flow (leaving the other parameters fixed) tends to increase reversal frequency (Kutzner and Christensen, 2004; Olson et al., 2010). In the evolving dynamo shown in Fig. 3b, the minimum heat flow was chosen to produce non-reversing conditions and the maximum heat flow was chosen to produce a reversal frequency near 6 Myr^{-1}, close to the post-CNS peak rate. The simulation began and ended in the non-reversing state, and these portions of the record are spliced and joined to produce a superchron of about 40 Myr duration.

Table 1 shows that $\omega_n = 0.476$ for the entire simulation in Fig. 3b, including all $n = 478$ reversals. This is more than 9 standard deviations above what is expected for uniformly random times, and demonstrates the strong modulation of reversals caused by the time-dependent core–mantle boundary heat flow. Because this dynamo started and ended in non-reversing states, the length of the superchron is arbitrary, and the choice of superchron length does have some affect on the overall ω_n. Accordingly, we also analyze reversal frequency statistics in this dynamo away from its

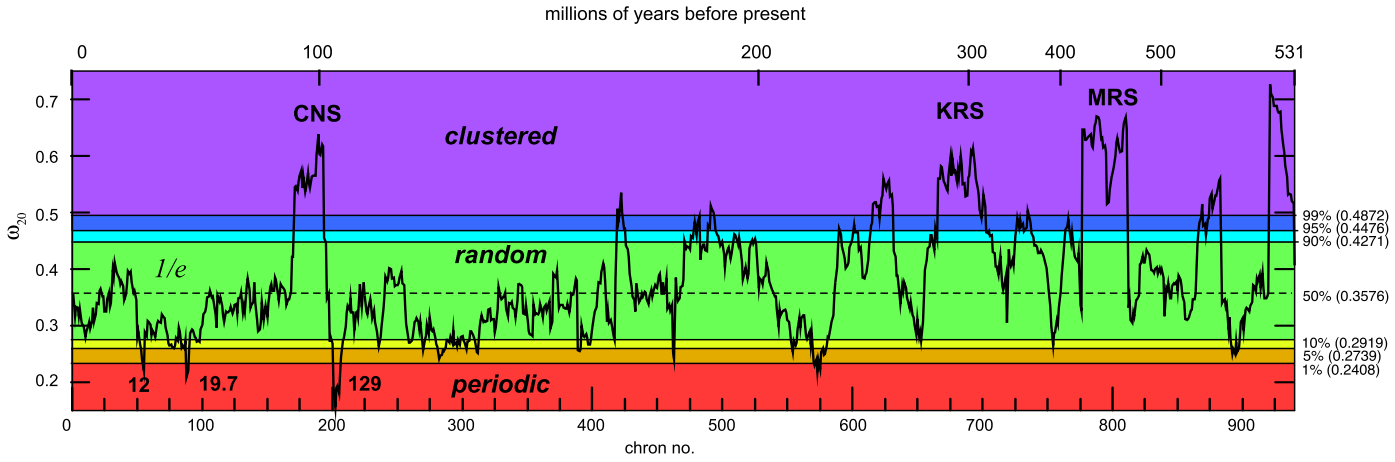

Fig. 4. Sherman's test for $n = 20$ reversals versus chron number for the Phanerozoic GPTS from Ogg (2012). Background colors denote Sherman percentiles for random times calculated as in Appendix A. Age in millions of years is shown on the top scale.

non-reversing state. Table 1 gives Sherman test results for this dynamo during the 80 Myr and 50 Myr reversing intervals prior to the superchron shown in Fig. 3b. For $n = 239$ reversals during the 80 Myr interval, we find $\omega_n = 0.4094$, which is nearly 2.6 standard deviations above what is expected for uniformly random times. As Table 1 shows, the Sherman test for this 80 Myr interval of the evolving dynamo are comparable to the Sherman test for 0–62 Ma from Ogg's (2012) 0–80 Ma GPTS, but unmistakably different from the Sherman test for the stationary dynamo. An even more direct comparison of the two dynamos uses 50 Myr intervals that include approximately the same number of reversals in each case. Table 1 shows that, over 50 Myr, ω_n for the evolving dynamo exceeds random behavior by 1.5 standard deviations, the same amount by which the stationary dynamo falls below random behavior.

In summary, the reversal sequence from our stationary dynamos has an overall ω-value somewhat lower than what is expected for uniformly random times, whereas long reversal sequences in the evolving dynamo are characterized by ω-values greater than what is expected for uniformly random times. For the evolving dynamo shown in Fig. 3b, the overall ω-value is similar to the entire GPTS, and it is also similar to the GPTS away from superchrons. These comparisons support (but do not prove) the interpretation that major reversal frequency variations in the GPTS are produced by fluctuations in the state of the geodynamo over Phanerozoic time.

5. Sherman's test on short reversal sequences

Further insights into geomagnetic reversal patterns come from analyzing shorter sequences of reversals in terms of ω, using either a sliding window with a fixed number of reversals, or alternatively, a sliding window with a fixed time span.

5.1. Reversal sequences with fixed number of chrons

Fig. 4 shows ω_{20} for Ogg's (2012) Phanerozoic GPTS as a function of chron number, calculated using a sliding window consisting of $n = 20$ reversals. The peaks in ω_{20} that correspond to the three Phanerozoic superchrons are labeled, and ages of several of the minima in ω_{20} are also labeled. Strong clustering as evidenced by large ω_{20} occurs around the three superchrons, but there is also some clustering around chrons 425 and 630. Evidence for nearly periodic behavior in the form of small ω_{20} occurs around chrons 55, 87, 200, and 575, respectively. However, in spite of these peaks and troughs, ω_{20} is close to μ_{20} as defined by (3) over much of the Phanerozoic. Additional tests with different n-values (not shown)

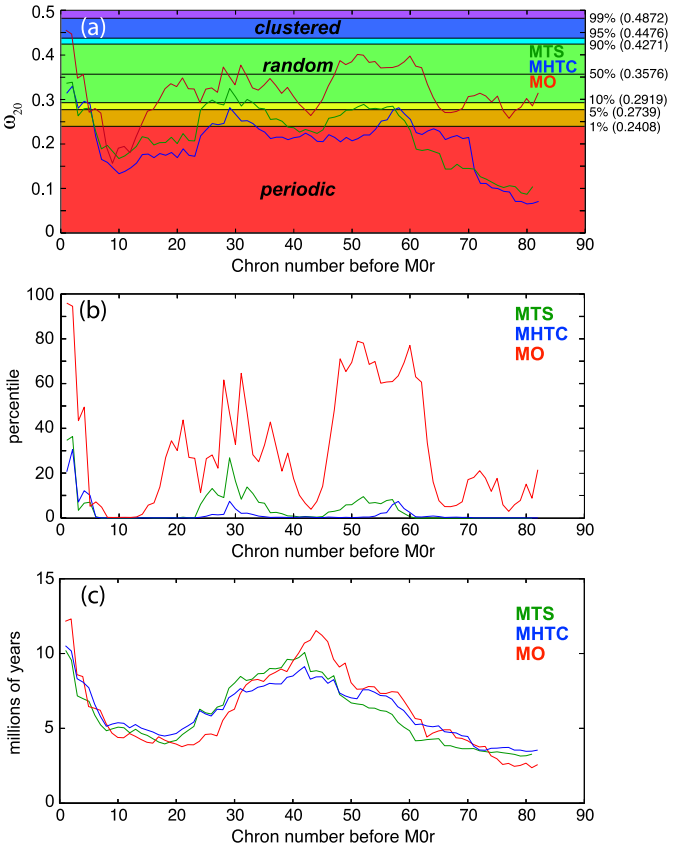

Fig. 5. Sherman's test for $n = 20$ reversals for the three Mesozoic M-sequences in Table 1. (a) ω_{20} versus chron number. MO = Ogg (2012); MTS = Tominga and Sager (2010); MHTC = Malinverno et al. (2012). Background colors denote Sherman percentiles for random times calculated as in Appendix A. (b) Sherman percentile versus chron number. (c) Duration of each $n = 20$ sequence versus chron number.

indicate that ω_n does not depend strongly on n, provided it is not much larger than 20. Accordingly, for many Phanerozoic sequences consisting of a small number of reversals, the reversal times approximate uniformly random events.

However, there are several exceptional times, where even short reversal sequences depart from randomness. As noted in the previous section, there is evidence that the youngest part of Mesozoic M-sequence is at least partially regular, and in places it appears to be highly regular. Fig. 5 shows ω_{20} for the three M-sequences, with the background colors indicating Sherman percentiles. For the

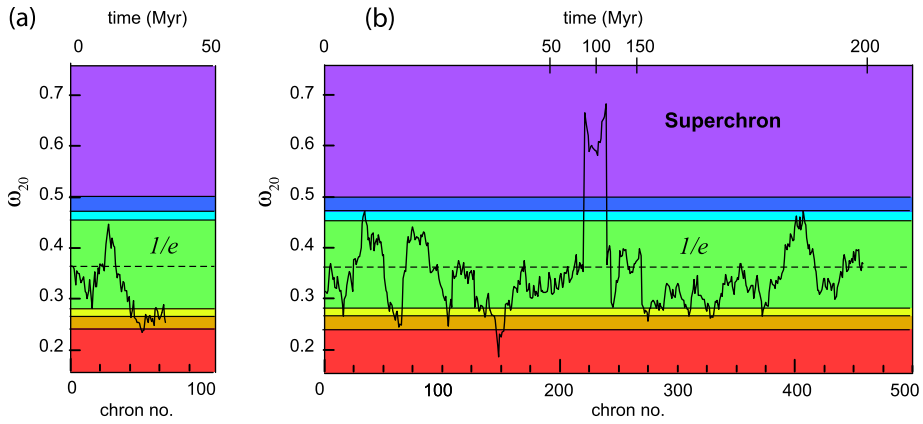

Fig. 6. Sherman's test for $n = 20$ reversals versus chron number for the numerical dynamos. (a) Dynamo with fixed parameters. (b) Dynamo with evolving parameters. Background colors denote the same Sherman percentiles as in Figs. 4 and 5.

MTS and MHTC compilations, ω_{20} falls below the 1% percentile around chron numbers M10–20, M40–55, and M70–80. In these sequences, each representing more than 5 Myr, the reversal times are nearly equally spaced.

Fig. 6 shows ω_{20} as a function of chron number for the numerical dynamos with evolving and fixed parameters, respectively, calculated with the same sliding window used in Figs. 4 and 5. The superchron in the evolving dynamo in Fig. 6 has a peak value of $\omega_{20} \simeq 0.65$, very close to the peak ω_{20}-values for the three GPTS superchrons in Fig. 4. In addition, the evolving dynamo shows a few sequences with low ω_{20}, which, like the low ω_{20} M-sequences in the GPTS, indicate periodic behavior. In contrast, the dynamo with fixed parameters in Fig. 6 is missing the large values of ω_{20} that signify strong clustering, although it does include a short sequence with low ω_{20}, indicative of periodic behavior.

5.2. Reversal sequences with fixed time span

Figs. 7a and 7b show Sherman percentiles for two segments of Ogg's (2012) GPTS, 124–224 Ma (pre-CNS) and 0–80 Ma (post-CNS), respectively, calculated as described in Appendix A, with a sliding window of length 5.45 Myr. Figs. 7c and 7d show results of the same test before and after the superchron of the evolving numerical dynamo. Fig. 7 also shows the number of reversals within each 5.45 Myr window. Larger values of P, approaching 100%, correspond to reversal clustering, whereas smaller values, those approaching 0%, correspond to periodic reversal behavior. Fig. 7 indicates the duration of the various fluctuations in reversal behavior. Qualitatively similar variations are evident in Fig. 7 from the evolving numerical dynamo. A striking property of this dynamo is the ~ 10 Myr alternation between high and low P-values, with essentially the same time scale of variations as in the GPTS. Given that $P \simeq 50\%$ corresponds to random reversal sequences, whereas low P corresponds to periodic reversal sequences, this constitutes evidence for 10 Myr geodynamo alternations between states with randomly timed reversals and reversals that occur with a more regular timing.

6. Conclusions

Sherman's ω-test offers clear-cut advantages for analyzing geomagnetic reversal times, in comparison with traditional approaches that rely on constructing and interpreting chron distribution functions. First, Sherman's test is easier to use. Second, it is applicable to relatively short reversal sequences because it is based on a small numbers statistic. Third and most importantly, it quantifies the deviation from uniformly distributed random times in terms of clustering versus periodicity, deviations from randomness that are found in reversing numerical dynamos.

Sherman's test demonstrates that the GPTS is not uniformly random. Instead, the GPTS fluctuates between sequences of clustered reversals, periodic reversals, and nearly uniformly random reversals. The ω_n for the entire Phanerozoic reversal record far exceeds that of a uniformly random sequence, due to clustering imposed largely by the three superchrons (CNS, KRS, MRS) with contributions from other parts of the Paleozoic record and the Cenozoic C-sequence, which has an ω-value 2.3 standard deviations above random. Reversals are nearly periodic in portions of the Mesozoic M-sequence, according to two recent chronologies, with Sherman statistics 2.6 to 4.2 standard deviations below the value expected for uniformly random times. In addition, Sherman's test applied to short reversal sequences ($n = 20$) from the GPTS reveals significant modulations through time, with clustering keyed to the three superchrons. Using a fixed 5.45 Myr time window, Sherman's test on the pre-CNS interval (125–205 Ma) and post-CNS interval (0–80 Ma) of the GPTS show alternation between periodic reversals and random reversals. The dominant time scales are the $\sim$200 Myr intervals between superchrons and the $\sim$10 Myr alternation between random and periodic behavior.

Similar variations are produced by a numerical dynamo with time-dependent control parameters, but are missing from the same dynamo with fixed control parameters. In spite of the fact that it is highly simplified and far from Earth-like in certain respects, the evolving dynamo produced both a superchron cycle and $\sim$10 Myr long alternations between periodic ($P \simeq 0$) and random ($P \simeq 50\%$) sequences that are remarkably like those in the GPTS (compare Figs. 7a, 7b to Figs. 7c, 7d), supporting our interpretation that long time scale GPTS variations reflect temporal changes in the state of the core, rather than being the outcome of time-independent dynamo processes.

The multiple time scales of variability in the GPTS are consistent with rapid but nonuniform evolution of the core. Estimates of the present-day heat loss from the core around 10–16 TW (Van der Hilst et al., 2007; Lay et al., 2008; Wu et al., 2011), coupled with upward estimates of the electrical and thermal conductivity of core metals (de Koker et al., 2012) imply rapid cooling, but other lines of evidence indicate that the rate of cooling of the core has been unsteady. In particular, dynamical reconstructions of the mantle (Zhang and Zhong, 2011) yield substantial temporal variations in core–mantle boundary heat flow, and the three-dimensional structure of the inner core suggests it has experienced time variations in its growth (Deguen and Cardin, 2009), indicating more variability in the history of the core than previously envisioned.

Acknowledgements

This research was supported by Frontiers in Earth System Dynamics grant EAR-1135382 from the National Science Foundation.

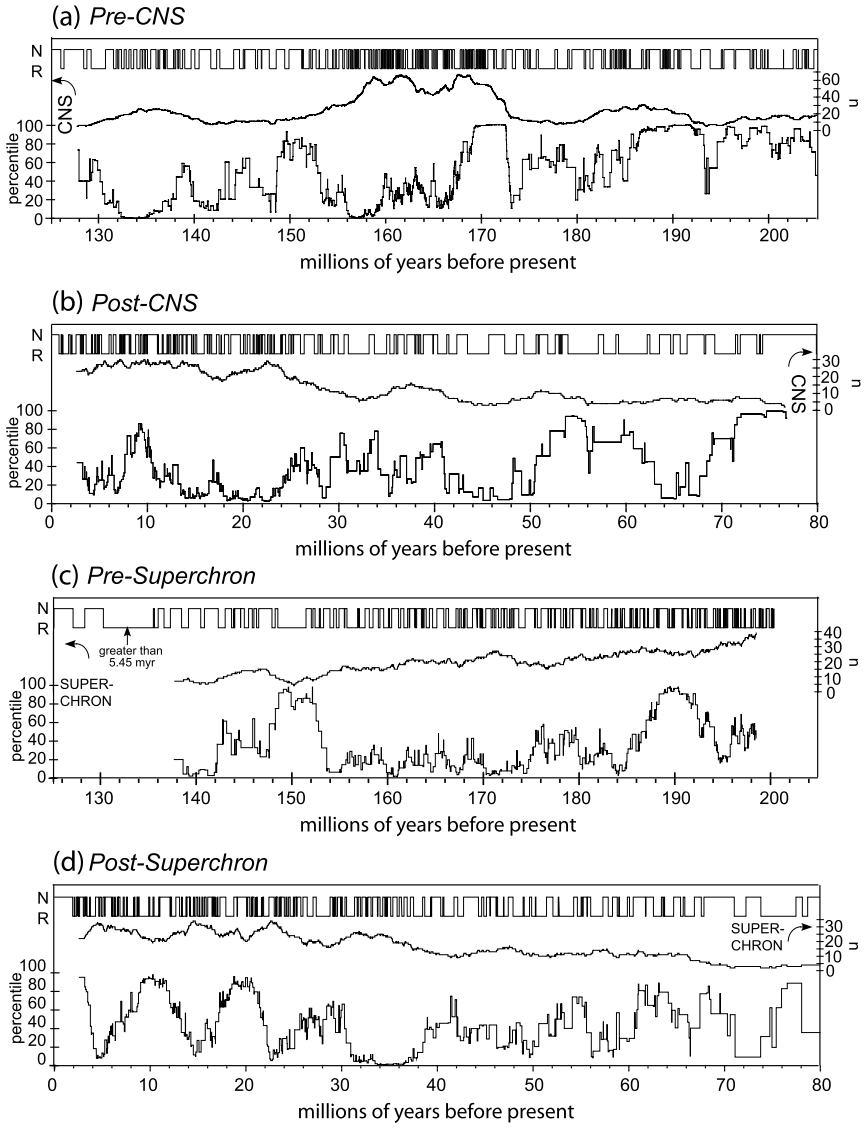

Fig. 7. Sherman percentiles versus age comparison: (a, b) pre-CNS and post-CNS, respectively, from Ogg's (2012) GPTS2012; (c, d) pre-superchron and post-superchron, respectively, from the evolving numerical dynamo. Each panel includes the polarity record (upper), the number of reversals n used in the calculation (middle), and the resulting Sherman percentile (lower).

We thank Jim Ogg (Purdue University) for providing the GPTS2012 in advance of publication, Chet Grosch (Old Dominion University) for pointing out the advantages of Sherman's test, and three referees for their helpful reviews.

Appendix A

The following expression derived by Sherman (1950) gives the probability that ω_n of n uniformly distributed random times is less than or equal to some number ω_0:

$$P(\omega_n \leqslant \omega_0) = 1 + \sum_{q=0}^{n-r-1} \sum_{p=0}^{q} (-1)^{q-p+1} \binom{n}{p} \binom{n+1}{q+1} \binom{n+q-p}{n} \times \left(\frac{n-q}{n+1}\right)^p \left(\frac{n-q}{n+1} - \omega_0\right)^{n-p} \quad \text{(A.1)}$$

where r is the non-negative integer satisfying

$$\frac{r}{n+1} \leqslant \omega_0 < \frac{r+1}{n+1}.$$

Table A1
Sherman percentiles for uniformly distributed random times.

n	$P = 99\%$	95%	90%
4	0.58870	0.50955	0.46850
5	0.57442	0.50181	0.46195
6	0.56263	0.49398	0.45847
7	0.55128	0.48801	0.45434
8	0.54241	0.48243	0.45100
9	0.53435	0.47772	0.44786
10	0.52743	0.47346	0.44510
11	0.52126	0.46970	0.44257
12	0.51577	0.46630	0.44029
13	0.51082	0.46323	0.43820
14	0.50634	0.46043	0.43628
15	0.50225	0.45786	0.43452
16	0.49851	0.45550	0.43288
17	0.49506	0.45332	0.43137
18	0.49188	0.45130	0.42995
19	0.48892	0.44942	0.42863
20	0.48617	0.44766	0.42739

Table A1 gives values of ω_0 that correspond to $P = 0.99, 0.95, 0.90$ (99%, 95%, and 90% percentiles) for $n = 4$ to $n = 20$, calculated by Sherman (1957) using (A.1).

Table A2
Errors in Sherman percentiles using Bartholomew's (1954) approximation.

n	$P = 99\%$	95%	90%
4	0.1%	0.6	1.5
6	0.1	0.3	0.8
10	0.1	0.1	0.3
20	0.0	0.0	0.1

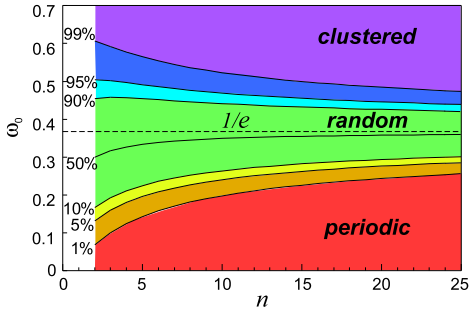

Fig. A1. Contour plot of Sherman percentiles as a function of n and ω_0.

Bartholomew (1954) derived the following approximation to (A.1), which we use in this paper:

$$P(\omega_n \leqslant \omega_0) \simeq \frac{1}{2}\left(1 + erf(z/\sqrt{2})\right) \tag{A.2}$$

where $erf(z)$ is the error function, and

$$z = z_1 - \frac{0.0995}{\sqrt{n}}\left(z_1^2 - 1\right)$$

with

$$z_1 = \frac{\omega_0 - 0.3679(1 - 0.5n^{-1})}{0.2431n^{-\frac{1}{2}}(1 - 0.605n^{-1})}.$$

Table A2 gives errors when calculating percentiles for small samples using the approximation (A.2) in place of (A.1). They are appreciable only for $n < 6$ and percentiles of 90% or less. For all other cases, (A.2) produces negligible error. Fig. A1 is a contour plot of P versus n and ω_0 using (A.2).

References

Amit, H., Leonhardt, R., Wicht, J., 2010. Polarity reversals from paleomagnetic observations and numerical dynamo simulations. Space Sci. Rev. 155, 293–335.

Aubert, J., Aurnou, J.M., Wicht, J., 2008. The magnetic structure of convection-driven numerical dynamos. Geophys. J. Int. 172 (3), 945–956.

Aubert, J., Labrosse, S., Poitou, C., 2009. Modeling the paleo-evolution of the geodynamo. Geophys. J. Int. 179, 1414–1428.

Bartholomew, J.T., 1954. Note on the use of Sherman's statistic as a test for randomness. Biometrika 41, 556–558.

Biggin, A.J., Steinberger, B., Aubert, J., Suttie, N., Holme, R., Torsvik, T.H., van der Meer, D.G., van Hinsbergen, D.J.J., 2012. Possible links between long-term geomagnetic variations and whole-mantle convection processes. Nat. Geosci. 5, 526–533.

Cande, S., Kent, D., 1995. Revised calibration of the geomagnetic polarity timescale for the late Cretaceous and Cenozoic. J. Geophys. Res., Solid Earth 100 (4), 6093–6095.

Carbone, V., Sorriso-Valvo, L., Vecchio, A., Lepreti, F., Veltri, P., Harabaglia, P., Guerra, I., 2006. Clustering of polarity reversals of the geomagnetic field. Phys. Rev. Lett. 96 (12), 128501.

Constable, C., 2000. On rates of occurrence of geomagnetic reversals. Phys. Earth Planet. Inter. 118 (3), 181–193.

Courtillot, V., Olson, P., 2007. Mantle plumes link magnetic superchrons to Phanerozoic mass depletion events. Earth Planet. Sci. Lett. 260 (3), 495–504.

de Koker, N., Steinle-Neumann, G., Vlcek, V., 2012. Electrical resistivity and thermal conductivity of liquid Fe alloys at high P and T, and heat flux in Earth's core. Proc. Natl. Acad. Sci. USA 109 (11), 4070–4073.

Deguen, R., Cardin, P., 2009. Tectonic history of the Earth's inner core preserved in its seismic structure. Nat. Geosci. 2 (6), 419–422.

Driscoll, P.E., Olson, P., 2009a. Effects of buoyancy and rotation on the polarity reversal frequency of gravitationally driven numerical dynamos. Geophys. J. Int. 178 (3), 1337–1350.

Driscoll, P.E., Olson, P., 2009b. Polarity reversals in geodynamo models with core evolution. Earth Planet. Sci. Lett. 282 (1–4), 24–33.

Driscoll, P.E., Olson, P., 2011. Superchron cycles driven by variable core heat flow. Geophys. Res. Lett. 38 (9), L09304.

Gallet, Y., Courtillot, V., 1995. Geomagnetic reversal behaviour since 100 Ma. Phys. Earth Planet. Inter. 92 (3), 235–244.

Gallet, Y., Hulot, G., 1997. Stationary and nonstationary behaviour within the geomagnetic polarity time scale. Geophys. Res. Lett. 24 (15), 1875–1878.

Glatzmaier, G.A., Coe, R.S., Hongre, L., Roberts, P.H., 1999. The role of the Earth's mantle in controlling the frequency of geomagnetic reversals. Nature 401, 885–890.

Hulot, G., Gallet, Y., 2003. Do superchrons occur without any palaeomagnetic warning?. Earth Planet. Sci. Lett. 210 (12), 191–201.

Jones, C.A., Thompson, M.J., Tobias, S.M., 2010. The solar dynamo. Space Sci. Rev. 152, 591–616.

Jonkers, A., 2003. Long-range dependence in the Cenozoic reversal record. Phys. Earth Planet. Inter. 135, 253–266.

Jonkers, A., 2007. Discrete scale invariance connects geodynamo timescales. Geophys. J. Int. 171 (2), 581–593.

Kutzner, C., Christensen, U.R., 2004. Simulated geomagnetic reversals and preferred virtual geomagnetic pole paths. Geophys. J. Int. 157 (3), 1105–1118.

Lay, T., Hernlund, J., Buffett, B.A., 2008. Core-mantle boundary heat flow. Nat. Geosci. 1 (1), 25–32.

Lhuillier, F., Hulot, G., Gallet, Y., 2013. Statistical properties of reversals and chrons in numerical dynamos and implications for the geodynamo. Phys. Earth Planet. Inter. 220, 19–36.

Lowrie, W., Kent, D., 1983. Geomagnetic reversal frequency since the Late Cretaceous. Earth Planet. Sci. Lett. 62, 305–313.

Lowrie, W., Kent, D., 2004. Geomagnetic polarity timescales and reversal frequency regimes. In: Chapman Conference on Timescales of the Internal Geomagnetic. Gainesville, Florida. In: Geophys. Monograph Series, vol. 145, pp. 117–129.

Malinverno, A., Hildebrandt, J., Tominaga, M., Channell, J.E.T., 2012. M-sequence geomagnetic polarity time scale (MHTC12) that steadies global spreading rates and incorporates astrochronolgy constraints. J. Geophys. Res. 117, B06104.

McFadden, P.L., 1984. Statistical tools for the analysis of geomagnetic reversal sequences. J. Geophys. Res. 89, 3363–3372.

McFadden, P.L., Merrill, R.T., 1984. Lower mantle convection and geomagnetism. J. Geophys. Res. 89, 3354–3362.

McFadden, P., Merrill, R., 1997. Asymmetry in the reversal rate before and after the Cretaceous Normal Polarity Superchron. Earth Planet. Sci. Lett. 149 (1–4), 43–47.

Naidu, P., 1971. Statistical structure of geomagnetic field reversals. J. Geophys. Res. 76 (11), 2649–2662.

Ogg, J.G., 2012. The geomagnetic polarity time scale. In: Gradstein, F.M., Ogg, J.G., Schmitz, M., Ogg, G. (Eds.), Geologic Time Scale 2012. Elsevier, pp. 85–114. Chapter 5.

Olson, P., Coe, R.S., Driscoll, P.E., Glatzmaier, G.A., Roberts, P.H., 2010. Geodynamo reversal frequency and heterogeneous core–mantle boundary heat flow. Phys. Earth Planet. Inter. 180, 66–79.

Olson, P., Glatzmaier, G.A., Coe, R.S., 2011. Complex polarity reversals in a geodynamo model. Earth Planet. Sci. Lett. 304 (1), 168–179.

Olson, P., Deguen, R., Hinnov, L.A., Zhong, S., 2013. Controls on geomagnetic reversals and core evolution by mantle convection in the Phanerozoic. Phys. Earth Planet. Inter. 214, 87–103.

Pavlov, V., Gallet, Y., 2005. A third superchron during the early Paleozoic. Episodes 28 (2), 78–84.

Phillips, J., 1977. Time variation and asymmetry in the statistics of geomagnetic reversal sequences. J. Geophys. Res. 82 (5), 835–843.

Ryan, D., Sarson, G., 2007. Are geomagnetic field reversals controlled by turbulence within the Earth's core?. Geophys. Res. Lett. 34, L02307. http://dx.doi.org/10.1029/2006GL028291. (6).

Shcherbakov, V., Fabian, K., 2012. The geodynamo as a random walker: A view on reversal statistics. J. Geophys. Res. 117, 3101.

Sherman, B., 1950. A random variable related to the spacing of sample values. Ann. Math. Stat. 21, 339–361.

Sherman, B., 1957. Percentiles of the ω_n statistic. Ann. Math. Stat. 28, 259–261.

Sorriso-Valvo, L., Stefani, F., Carbone, V., Nigro, G., Lepreti, F., Ceccio, A., Veltri, P., 2007. A statistical analysis of polarity reversals of the geomagnetic field. Phys. Earth Planet. Inter. 164, 197–207.

Tominaga, M., Sager, W.W., 2010. Revised Pacific M-anomaly geomagnetic polarity timescale. Geophys. J. Int. 182, 203–232.

Van der Hilst, R.D., De Hoop, M.V., Wang, P., Shim, S.H., Ma, P., Tenorio, L., 2007. Seismostratigraphy and thermal structure of Earth's core–mantle boundary region. Science 315 (5820), 1813–1817.

Valet, J.-P., Plenier, G., Herrero-Bervera, E., 2008. Geomagnetic excursions reflect an aborted polarity state. Earth Planet. Sci. Lett. 274, 472–478.

Valet, J.-P., Fournier, A., Courtillot, V., Herrero-Bervera, E., 2012. Dynamical similarity of geomagnetic field reversals. Nature 490 (7418), 89–93.

Vallianatos, F., 2011. A non-extensive statistical physics approach to the polarity reversals of the geomagnetic field. Physica A 390 (10), 1773–1778.
Wicht, J., Olson, P., 2004. A detailed study of the polarity reversal mechanism in a numerical dynamo model. Geochem. Geophys. Geosyst. 5 (3).
Wicht, J., Stellmach, S., Harder, H., 2009. Numerical models of the geodynamo: From Fundamental Cartesian Models to 3D simulations of field reversals. In: Glazmeier, K.-H., Soel, H., Negendank, J.F.W. (Eds.), Geomagnetic Field Variations. Springer, pp. 107–158.
Wicht, J., Stellmach, S., Harder, H., 2010. Numerical dynamo simulations: From basic concepts to realistic models. In: Freeden, W., Nashed, M.Z., Sonar, T. (Eds.), Handbook of Geomathematics. Springer, Berlin Heidelberg, pp. 459–502.
Wu, B., Driscoll, P., Olson, P., 2011. A statistical boundary layer model for the mantle D'' region. J. Geophys. Res., Solid Earth (1978–2012) 116 (B12).
Zhang, N., Zhong, S., 2011. Heat fluxes at the Earth's surface and core–mantle boundary since Pangea formation and their implications for the geomagnetic superchrons. Earth Planet. Sci. Lett. 306 (3), 205–216.